Multi-Resolution Bayesian Compressive Sensing for Sparse Target Inversion

M. Salucci, L. Poli, F. Zardi, L.Tosi, S. Lusa, and A. Massa

2025/03/28

Contents

1 Basic Formulation

Let us consider an inaccessible investigation domain Λ irradiated by a set of incident transverse-magnetic planes $E^v_{inc}(\mathbf{r}^v)$, $v = 1, ..., V$, impinging from the angular directions $\theta^v = \frac{2\pi}{V}(v-1)$, being V the number of views. In this working scenario, the scattered field $E^v_{scatt}(\mathbf{r}^v_s)$, $s = 1, ..., S$, is supposed to be measured through a set of S sensors equally displaced on a circular observation domain Θ, external to the investigation domain ($\Lambda \cap \Theta = 0$), having radius ρ. The exact location of the sensors are identified by the position vector $\mathbf{r}^v_s = (\rho \cos\theta^v_s \sin\theta^v_s)$, being $\theta^v_s = \theta^v + \frac{2\pi}{S}(s-1)$. This scattered field is known to be dependent on the equivalent currents $J^v_{eq}(\mathbf{r})$ generated in the support of the unknown scatterers placed into the domain Λ, according to the *data equation*

$$E^v_{scatt}(\mathbf{r}^v_s) = -k_0^2 \int_{\Lambda} J^v_{eq}(\mathbf{r}')\, G(\mathbf{r}^v_s/\mathbf{r}') \tag{1}$$

where $G(\mathbf{r}^v_s/\mathbf{r}')$ is the Green's function in the fre space and $k_0 = \omega\sqrt{\varepsilon_0\mu_0}$. The material propertiesof the investigation domain Λ in terms of relative dielectric permittivity $\varepsilon_r(\mathbf{r})$ and electric conductivity $\sigma(\mathbf{r})$ are described by means of the object function $\tau(\mathbf{r}) = \varepsilon_r(\mathbf{r}) - \varepsilon_0 - \frac{\sigma(\mathbf{r})}{2\pi f \varepsilon_0}$, being f the frequency of the TM plane wave. In order to numerically deal with (1), the investigation domain is discretized into N sub-domains (cells) by means of the Richmond's procedure, providing the matrix form of $\mathbf{E}^v = \mathbf{G}\mathbf{J}^v_{eq} + \mathbf{N}^v$, being G the Green's matrix and $\mathbf{N}^v$ the zero mean additive gaussian noise vector of variance σ^2. The dielectric features of the N sub-domains described through the discretized form of the object function τ, are then retrieved through the following iterative strategy which combines a multi-resolution approach and the BCS method, aimed to maximize the a-posteriori probability of the equivalent souces given the scattered field as:

$$\widehat{\mathbf{J}}^v_{eq} = \arg\left\{\max\left[\mathcal{P}\left(\mathbf{J}^v_{eq}\middle|\, \mathbf{E}^v_{scatt}\right)\right]\right\}, \qquad v = 1, ..., V \tag{2}$$

More in detail, the algorithms works as follows:

1. *Initialization*: Definition of input parameters of the BCS problem, namely the initial estimation of the noise on the scattered data, σ^2_{init}, and the convergence parameter, γ, and the parameter related to the stopping criterion of the $IMSA$, χ. Set the region of interest equal to the whole domain $\mathcal{D}^{(1)} = \Lambda$;

2. *BCS inversion via "Constrained-RVM"*:
   (a) increase of the iteration index: $i = i + 1$;
   (b) solution of the BCS problem within the Region of Interest (*RoI*) $\mathcal{D}^{(i-1)}$ defined at the $(i-1)$-th step, by maximizing the following cost function:

$$\ell(\mathbf{a}^v) = -0.5\left[2S\log(2\pi) + \log(\mathbf{C}) + \left(\mathbf{E}^v_{scatt}\right)^T \mathbf{C}^{-1}\left(\mathbf{E}^v_{scatt}\right)\right], \qquad v = 1, ..., V \tag{3}$$

   where $\mathbf{C} = \sigma^2\mathbf{I} + \mathbf{G}\left[diag(\mathbf{a}^v)\right]^{-1}\mathbf{G}^T$ and being $\mathbf{a}^v$ the hyperparameter vector whose entries corresponding to the cells out of the *RoI* $\mathcal{D}^{(i-1)}$ are forced to ∞;

3. *Equivalent Current Retrieval*:

Computation of the equivalent currents starting from the hyperparameter vector $\mathbf{a}^v$ according to:

$$\mathbf{J}_{eq}^{v} = \frac{1}{\sigma^2}\left[\frac{\mathbf{G}^T\mathbf{G}}{\sigma^2} diag\left(\mathbf{a}^v\right)\right]^{-1}\mathbf{G}^T\mathbf{E}_{scatt}^{v}, \qquad v = 1, ..., V \tag{4}$$

4. *Features' Retrieval*:

   Reconstruction of the material properties of the investigation domain taking advantage from the first order Born approximation through

$$\tau\left(\mathbf{r}_n^{(i)}\right) = \frac{1}{V}\sum \frac{\mathbf{J}_{eq}^{v}\left(\mathbf{r}_n^{(i)}\right)}{\mathbf{E}_{inc}^{v}\left(\mathbf{r}_n^{(i)}\right) + \sum_{p=1}^{N}\mathbf{J}_{eq}^{v}\left(\mathbf{r}_n^{(i)}\right)\left[\int_D \mathbf{Gr}\right]}, \qquad n = 1, ..., N \tag{5}$$

   being $\mathbf{r}_n^{(i)}$ the barycenter of the n-th cell within the *RoI* $\mathcal{D}^{(i-1)}$;

5. *Convergence Check*:

   Definition of the new *RoI* $\mathcal{D}^{(i)}$ according to the contrast function distribution calculated with (5) and evaluation of the following termination condition:

$$\left(\frac{L^{(i-1)} - L^{(i)}}{L^{(i)}}\right) < \chi \tag{6}$$

   being $L^{(i)}$ the side of the *RoI* $\mathcal{D}^{(i)}$. If (6) is met, then stop the iterative process otherwise go to step 2.

2 Analysis with Different Object Shapes - Domain $L = 6.0\lambda$

2.1 E-shaped Object, $\ell = 1.5\lambda$

Test Case Description

Direct solver:

- Side of the investigation domain: $L = 6.0\lambda$
- Cubic domain divided in $\sqrt{D} \times \sqrt{D}$ cells
- Number of cells for the direct solver: $D = 1600$ (discretization $= \lambda/10$)

Investigation domain:

- Cubic domain divided in $\sqrt{N} \times \sqrt{N}$ cells
- Number of cells for the inversion:

  - First Step IMSA: $N^{(1)} = 100$ (discretization $= \lambda/10$)

  - Following Steps IMSA: $N^{(i)}$ not fixed, defined according to the estimated *RoI* $\mathcal{D}^{(i)}$

Measurement domain:

- Total number of measurements: $M = 60$
- Measurement points placed on circles of radius $\rho = 4.5\lambda$

Sources:

- Plane waves
- Number of views: $V = 60$; $\theta^{v}_{inc} = 0 + (v - 1) \times (360/V)$
- Amplitude: $A = 1.0$
- Frequency: $F = 300$ MHz ($\lambda = 1$)

Background:

- $\varepsilon_r = 1.0$
- $\sigma = 0$ [S/m]

Scatterer

- E-shaped object, $\ell = 1.5\lambda$
- $\varepsilon_r \in \{1.05,\ 1.10,\ 1.15, 1.20,\ 1.50,\ 2.00,\ 2.50\}$
- $\sigma = 0$ [S/m]

2.1.1 E-shaped Object, $\ell = 1.5\lambda$, $\tau = 0.10$ - IMSA-BCS reconstructed profiles

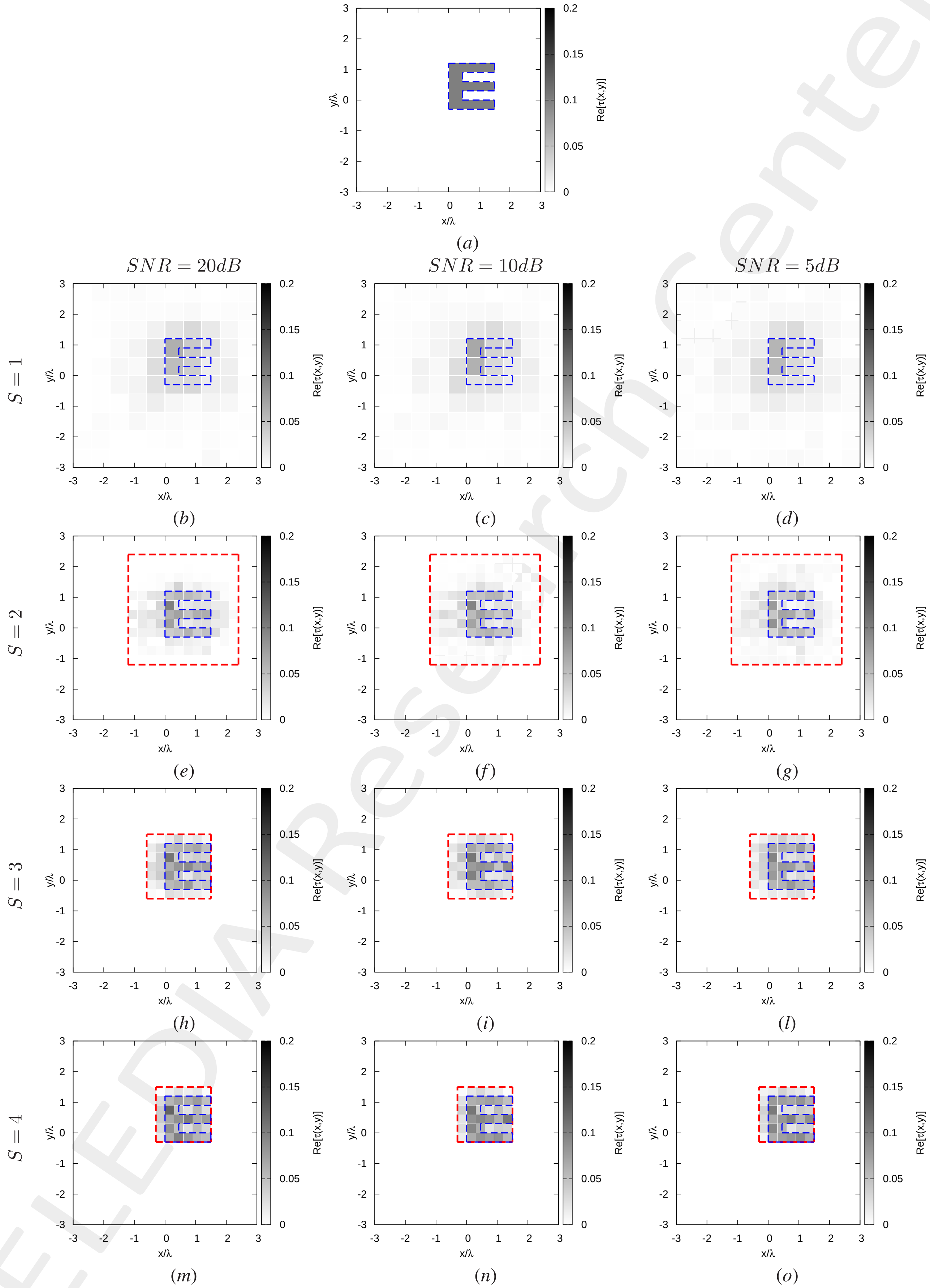

Figure 1: *E-shaped Object*, $\tau = 0.10$ - (a) Actual profile and (b)-(o) IMSA-BCS reconstructed profiles for $(b)(e)(h)(m)$ $SNR = 20$ [dB], $(c)(f)(i)(n)$ $SNR = 10$ [dB] and $(d)(g)(l)(o)$ $SNR = 5$ [dB] at the step (b)-(d) $S = 1$, (e)-(g) $S = 2$, (h)-(l) $S = 3$ and (m)-(o) $S = 4$.

	$SNR = 50dB$			
	$S = 1$	$S = 2$	$S = 3$	$S = 4$
ξ_{tot}	7.65×10^{-3}	4.04×10^{-3}	3.14×10^{-3}	2.38×10^{-3}
ξ_{int}	5.25×10^{-2}	4.12×10^{-2}	3.22×10^{-2}	2.57×10^{-2}
ξ_{ext}	5.29×10^{-3}	2.17×10^{-3}	1.69×10^{-3}	1.20×10^{-3}
	$SNR = 20dB$			
	$S = 1$	$S = 2$	$S = 3$	$S = 4$
ξ_{tot}	7.73×10^{-3}	4.08×10^{-3}	3.15×10^{-3}	2.50×10^{-3}
ξ_{int}	5.36×10^{-2}	4.17×10^{-2}	3.20×10^{-2}	2.61×10^{-2}
ξ_{ext}	5.31×10^{-3}	2.21×10^{-3}	1.71×10^{-3}	1.31×10^{-3}
	$SNR = 10dB$			
	$S = 1$	$S = 2$	$S = 3$	$S = 4$
ξ_{tot}	7.85×10^{-3}	4.16×10^{-3}	3.15×10^{-3}	2.27×10^{-3}
ξ_{int}	5.37×10^{-2}	4.14×10^{-2}	3.12×10^{-2}	2.30×10^{-2}
ξ_{ext}	5.39×10^{-3}	2.24×10^{-3}	1.73×10^{-3}	1.20×10^{-3}
	$SNR = 5dB$			
	$S = 1$	$S = 2$	$S = 3$	$S = 4$
ξ_{tot}	8.38×10^{-3}	4.42×10^{-3}	3.13×10^{-3}	2.22×10^{-3}
ξ_{int}	5.66×10^{-2}	4.30×10^{-2}	3.07×10^{-2}	2.15×10^{-2}
ξ_{ext}	5.78×10^{-3}	2.37×10^{-3}	1.74×10^{-3}	1.21×10^{-3}

Table I: *E-shaped Object,* $\tau = 0.10$ - Reconstrution errors: total (ξ_{tot}), internal (ξ_{int}) and external (ξ_{ext}) errors.

	$SNR = 50dB$			
	$S = 1$	$S = 2$	$S = 3$	$S = 4$
$L^{(S)}$	6.00	3.60	2.10	1.80
$N^{(S)}$	100	208	208	208
$Q^{(S)}$	100	144	49	36
	$SNR = 20dB$			
	$S = 1$	$S = 2$	$S = 3$	$S = 4$
$L^{(S)}$	6.00	3.60	2.10	1.80
$N^{(S)}$	100	208	208	208
$Q^{(S)}$	100	144	49	36
	$SNR = 10dB$			
	$S = 1$	$S = 2$	$S = 3$	$S = 4$
$L^{(S)}$	6.00	3.60	2.10	1.80
$N^{(S)}$	100	208	208	208
$Q^{(S)}$	100	144	49	36
	$SNR = 5dB$			
	$S = 1$	$S = 2$	$S = 3$	$S = 4$
$L^{(S)}$	6.00	3.60	2.40	2.10
$N^{(S)}$	100	208	208	208
$Q^{(S)}$	100	144	64	49

Table II: *E-shaped Object,* $\tau = 0.10$ - Investigation domain parameters: restricted investigation domain size $L^{(S)}$, total number of cells $N^{(S)}$ and number of cells within the restricted domain size $Q^{(S)}$.

2.1.2 E-shaped Object, $\ell = 1.5\lambda$, $\tau = 0.20$ - IMSA-BCS reconstructed profiles

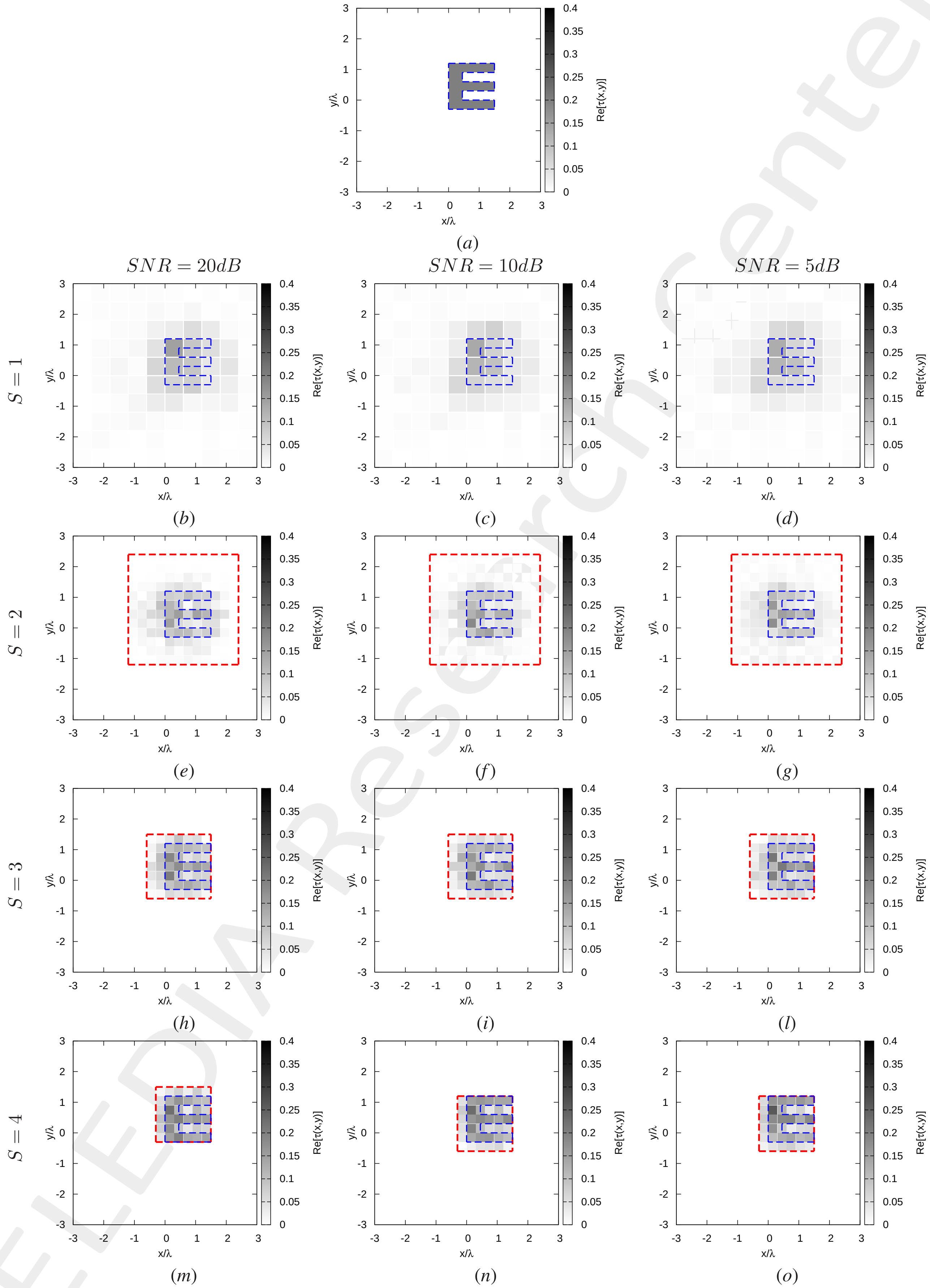

Figure 2: *E-shaped Object,* $\tau = 0.20$ - (a) Actual profile and (b)-(o) IMSA-BCS reconstructed profiles for $(b)(e)(h)(m)$ $SNR = 20$ [dB], $(c)(f)(i)(n)$ $SNR = 10$ [dB] and $(d)(g)(l)(o)$ $SNR = 5$ [dB] at the step (b)-(d) $S = 1$, (e)-(g) $S = 2$, (h)-(l) $S = 3$ and (m)-(o) $S = 4$.

	$SNR = 50dB$			
	$S = 1$	$S = 2$	$S = 3$	$S = 4$
ξ_{tot}	1.57×10^{-2}	8.80×10^{-3}	6.46×10^{-3}	4.23×10^{-3}
ξ_{int}	8.62×10^{-2}	8.46×10^{-2}	6.11×10^{-2}	3.86×10^{-2}
ξ_{ext}	1.17×10^{-2}	4.91×10^{-3}	3.70×10^{-3}	2.40×10^{-3}
	$SNR = 20dB$			
	$S = 1$	$S = 2$	$S = 3$	$S = 4$
ξ_{tot}	1.60×10^{-2}	8.89×10^{-3}	6.59×10^{-3}	4.82×10^{-3}
ξ_{int}	8.85×10^{-2}	8.55×10^{-2}	6.13×10^{-2}	4.38×10^{-2}
ξ_{ext}	1.19×10^{-2}	4.96×10^{-3}	3.80×10^{-3}	2.81×10^{-3}
	$SNR = 10dB$			
	$S = 1$	$S = 2$	$S = 3$	$S = 4$
ξ_{tot}	1.65×10^{-2}	8.45×10^{-3}	6.50×10^{-3}	4.45×10^{-3}
ξ_{int}	9.33×10^{-2}	7.78×10^{-2}	6.03×10^{-2}	4.03×10^{-2}
ξ_{ext}	1.19×10^{-2}	4.72×10^{-3}	3.80×10^{-3}	2.55×10^{-3}
	$SNR = 5dB$			
	$S = 1$	$S = 2$	$S = 3$	$S = 4$
ξ_{tot}	1.76×10^{-2}	9.26×10^{-3}	6.40×10^{-3}	4.62×10^{-3}
ξ_{int}	9.51×10^{-2}	8.35×10^{-2}	5.92×10^{-2}	4.36×10^{-2}
ξ_{ext}	1.28×10^{-2}	5.09×10^{-3}	3.55×10^{-3}	2.61×10^{-3}

Table III: *E-shaped Object,* $\tau = 0.20$ - Reconstrution errors: total (ξ_{tot}), internal (ξ_{int}) and external (ξ_{ext}) errors.

	$SNR = 50dB$			
	$S = 1$	$S = 2$	$S = 3$	$S = 4$
$L^{(S)}$	6.00	2.10	1.80	1.80
$N^{(S)}$	100	208	208	208
$Q^{(S)}$	100	144	49	36
	$SNR = 20dB$			
	$S = 1$	$S = 2$	$S = 3$	$S = 4$
$L^{(S)}$	6.00	2.10	1.80	1.80
$N^{(S)}$	100	208	208	208
$Q^{(S)}$	100	144	49	36
	$SNR = 10dB$			
	$S = 1$	$S = 2$	$S = 3$	$S = 4$
$L^{(S)}$	6.00	2.10	1.80	1.80
$N^{(S)}$	100	208	208	208
$Q^{(S)}$	100	144	49	36
	$SNR = 5dB$			
	$S = 1$	$S = 2$	$S = 3$	$S = 4$
$L^{(S)}$	6.00	2.10	1.80	1.80
$N^{(S)}$	100	208	208	208
$Q^{(S)}$	100	144	49	36

Table IV: *E-shaped Object,* $\tau = 0.20$ - Investigation domain parameters: restricted investigation domain size $L^{(S)}$, total number of cells $N^{(S)}$ and number of cells within the restricted domain size $Q^{(S)}$.

2.1.3 E-shaped Object, $\ell = 1.5\lambda$, $\tau = 0.50$ - IMSA-BCS reconstructed profiles

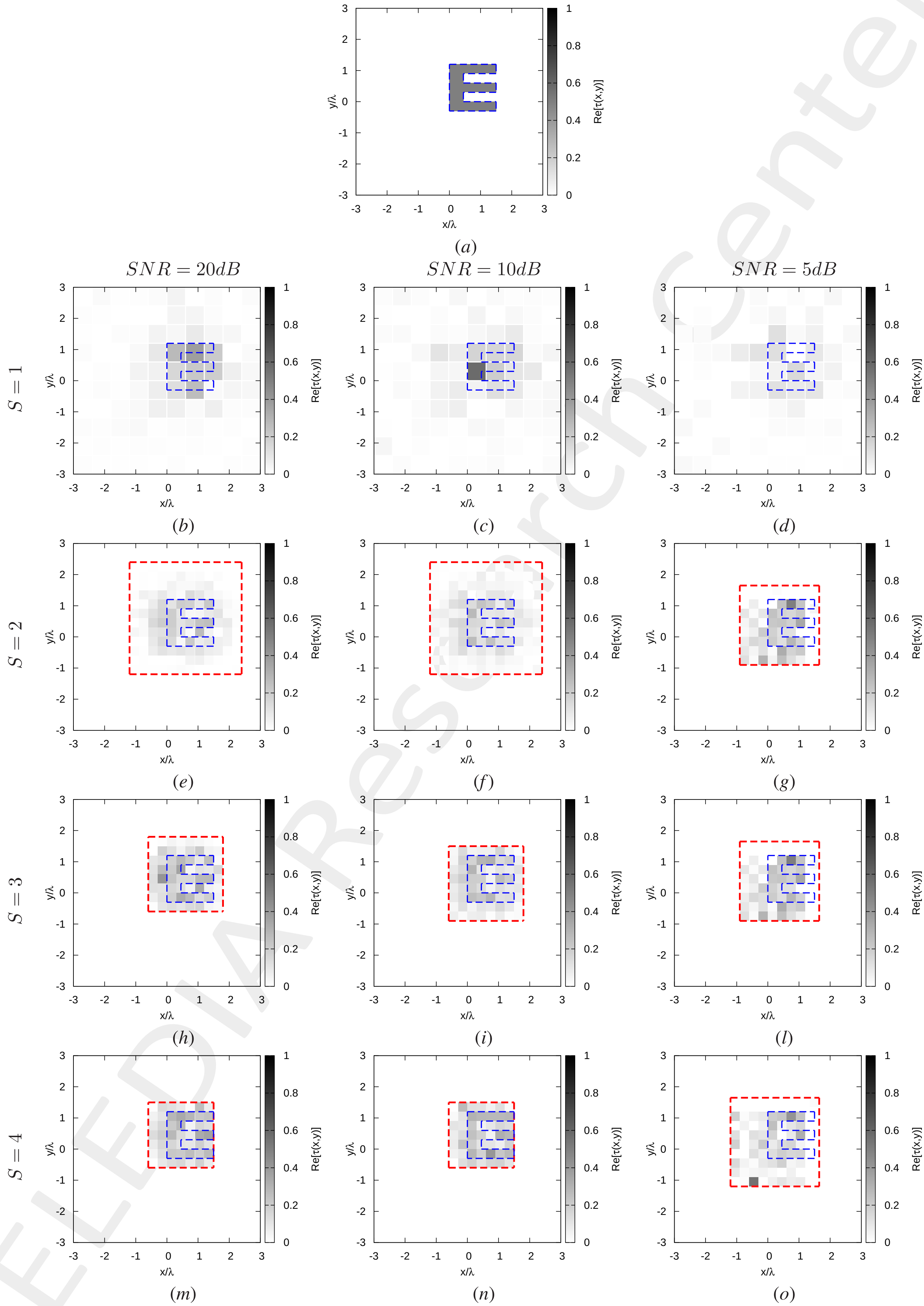

Figure 3: *E-shaped Object*, $\tau = 0.50$ - (a) Actual profile and (b)-(o) IMSA-BCS reconstructed profiles for $(b)(e)(h)(m)$ $SNR = 20$ [dB], $(c)(f)(i)(n)$ $SNR = 10$ [dB] and $(d)(g)(l)(o)$ $SNR = 5$ [dB] at the step (b)-(d) $S = 1$, (e)-(g) $S = 2$, (h)-(l) $S = 3$ and (m)-(o) $S = 4$.

	$SNR=50dB$			
	$S=1$	$S=2$	$S=3$	$S=4$
ξ_{tot}	4.03×10^{-2}	2.25×10^{-2}	1.98×10^{-2}	1.65×10^{-2}
ξ_{int}	1.91×10^{-1}	2.24×10^{-1}	1.97×10^{-1}	1.64×10^{-1}
ξ_{ext}	2.60×10^{-2}	1.15×10^{-2}	1.03×10^{-2}	8.76×10^{-3}
	$SNR=20dB$			
	$S=1$	$S=2$	$S=3$	$S=4$
ξ_{tot}	3.79×10^{-2}	2.32×10^{-2}	2.14×10^{-2}	1.76×10^{-2}
ξ_{int}	1.90×10^{-1}	2.29×10^{-1}	1.92×10^{-1}	1.76×10^{-1}
ξ_{ext}	2.55×10^{-2}	1.19×10^{-2}	1.18×10^{-2}	9.07×10^{-3}
	$SNR=10dB$			
	$S=1$	$S=2$	$S=3$	$S=4$
ξ_{tot}	4.18×10^{-2}	2.53×10^{-2}	1.96×10^{-2}	1.72×10^{-2}
ξ_{int}	2.06×10^{-1}	2.22×10^{-1}	1.99×10^{-1}	1.72×10^{-1}
ξ_{ext}	2.48×10^{-2}	1.36×10^{-2}	1.00×10^{-2}	8.78×10^{-3}
	$SNR=5dB$			
	$S=1$	$S=2$	$S=3$	$S=4$
ξ_{tot}	4.94×10^{-2}	2.75×10^{-2}	2.75×10^{-2}	2.75×10^{-2}
ξ_{int}	2.77×10^{-1}	3.33×10^{-1}	3.33×10^{-1}	3.33×10^{-1}
ξ_{ext}	2.73×10^{-2}	1.12×10^{-2}	1.12×10^{-2}	1.12×10^{-2}

Table V: *E-shaped Object,* $\tau=0.50$ - Reconstrution errors: total (ξ_{tot}), internal (ξ_{int}) and external (ξ_{ext}) errors.

	$SNR=50dB$			
	$S=1$	$S=2$	$S=3$	$S=4$
$L^{(S)}$	6.00	2.40	2.10	2.10
$N^{(S)}$	100	208	208	208
$Q^{(S)}$	100	144	64	49
	$SNR=20dB$			
	$S=1$	$S=2$	$S=3$	$S=4$
$L^{(S)}$	6.00	2.40	2.10	2.10
$N^{(S)}$	100	208	208	208
$Q^{(S)}$	100	144	64	49
	$SNR=10dB$			
	$S=1$	$S=2$	$S=3$	$S=4$
$L^{(S)}$	6.00	2.40	2.10	2.10
$N^{(S)}$	100	208	208	208
$Q^{(S)}$	100	144	64	49
	$SNR=5dB$			
	$S=1$	$S=2$	$S=3$	$S=4$
$L^{(S)}$	6.00	1.19	1.19	1.19
$N^{(S)}$	100	112	112	112
$Q^{(S)}$	100	16	16	16

Table VI: *E-shaped Object,* $\tau=0.50$ - Investigation domain parameters: restricted investigation domain size $L^{(S)}$, total number of cells $N^{(S)}$ and number of cells within the restricted domain size $Q^{(S)}$.

2.1.4 E-shaped Object, $\ell = 1.5\lambda$, $\tau = 1.00$ - IMSA-BCS reconstructed profiles

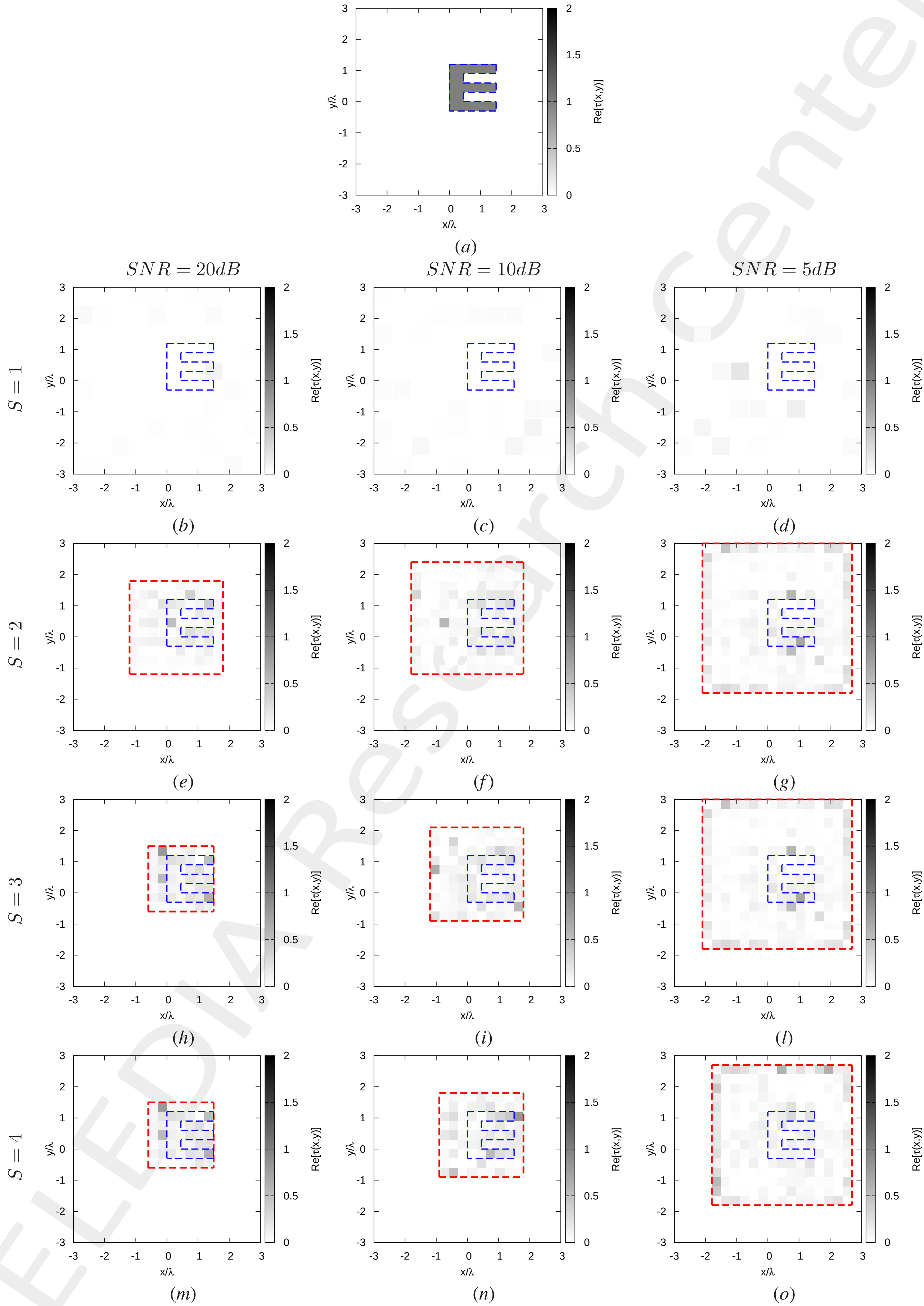

Figure 4: *E-shaped Object*, $\tau = 1.00$ - (*a*) Actual profile and (*b*)-(*o*) IMSA-BCS reconstructed profiles for (*b*)(*e*)(*h*)(*m*) $SNR = 20$ [dB], (*c*)(*f*)(*i*)(*n*) $SNR = 10$ [dB] and (*d*)(*g*)(*l*)(*o*) $SNR = 5$ [dB] at the step (*b*)-(*d*) $S = 1$, (*e*)-(*g*) $S = 2$, (*h*)-(*l*) $S = 3$ and (*m*)-(*o*) $S = 4$.

	$SNR = 50dB$			
	$S = 1$	$S = 2$	$S = 3$	$S = 4$
ξ_{tot}	6.39×10^{-2}	4.14×10^{-2}	3.35×10^{-2}	3.15×10^{-2}
ξ_{int}	5.89×10^{-1}	4.29×10^{-1}	4.39×10^{-1}	4.36×10^{-1}
ξ_{ext}	3.07×10^{-2}	1.66×10^{-2}	1.11×10^{-2}	8.13×10^{-3}
	$SNR = 20dB$			
	$S = 1$	$S = 2$	$S = 3$	$S = 4$
ξ_{tot}	6.11×10^{-2}	3.96×10^{-2}	3.29×10^{-2}	3.29×10^{-2}
ξ_{int}	5.63×10^{-1}	4.41×10^{-1}	4.11×10^{-1}	4.11×10^{-1}
ξ_{ext}	2.78×10^{-2}	1.43×10^{-2}	1.10×10^{-2}	1.10×10^{-2}
	$SNR = 10dB$			
	$S = 1$	$S = 2$	$S = 3$	$S = 4$
ξ_{tot}	6.47×10^{-2}	4.68×10^{-2}	4.55×10^{-2}	4.47×10^{-2}
ξ_{int}	5.60×10^{-1}	4.43×10^{-1}	4.43×10^{-1}	4.26×10^{-1}
ξ_{ext}	3.21×10^{-2}	2.01×10^{-2}	1.86×10^{-2}	1.92×10^{-2}
	$SNR = 5dB$			
	$S = 1$	$S = 2$	$S = 3$	$S = 4$
ξ_{tot}	1.29×10^{-1}	8.10×10^{-2}	7.34×10^{-2}	7.44×10^{-2}
ξ_{int}	5.58×10^{-1}	4.81×10^{-1}	4.58×10^{-1}	4.63×10^{-1}
ξ_{ext}	8.29×10^{-2}	4.64×10^{-2}	3.98×10^{-2}	4.58×10^{-2}

Table VII: *E-shaped Object,* $\tau = 1.00$ - Reconstrution errors: total (ξ_{tot}), internal (ξ_{int}) and external (ξ_{ext}) errors.

	$SNR = 50dB$			
	$S = 1$	$S = 2$	$S = 3$	$S = 4$
$L^{(S)}$	6.00	2.40	2.10	1.80
$N^{(S)}$	100	175	175	175
$Q^{(S)}$	100	100	64	49
	$SNR = 20dB$			
	$S = 1$	$S = 2$	$S = 3$	$S = 4$
$L^{(S)}$	6.00	2.10	2.10	2.10
$N^{(S)}$	100	175	175	175
$Q^{(S)}$	100	100	49	49
	$SNR = 10dB$			
	$S = 1$	$S = 2$	$S = 3$	$S = 4$
$L^{(S)}$	6.00	3.00	2.69	2.69
$N^{(S)}$	100	208	208	208
$Q^{(S)}$	100	144	100	81
	$SNR = 5dB$			
	$S = 1$	$S = 2$	$S = 3$	$S = 4$
$L^{(S)}$	6.00	5.10	4.80	4.50
$N^{(S)}$	100	343	343	343
$Q^{(S)}$	100	324	289	256

Table VIII: *E-shaped Object,* $\tau = 1.00$ - Investigation domain parameters: restricted investigation domain size $L^{(S)}$, total number of cells $N^{(S)}$ and number of cells within the restricted domain size $Q^{(S)}$.

2.1.5 E-shaped Object, $\ell = 1.5\lambda$ - Resume: Errors vs. τ

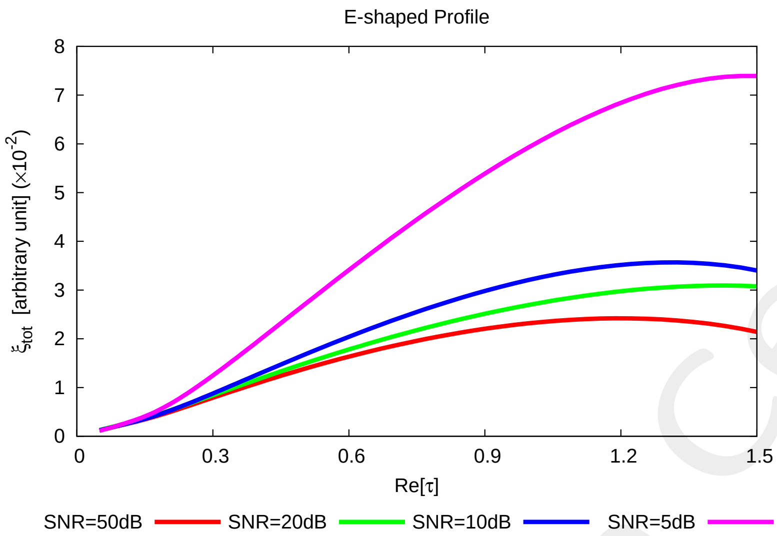

(a)

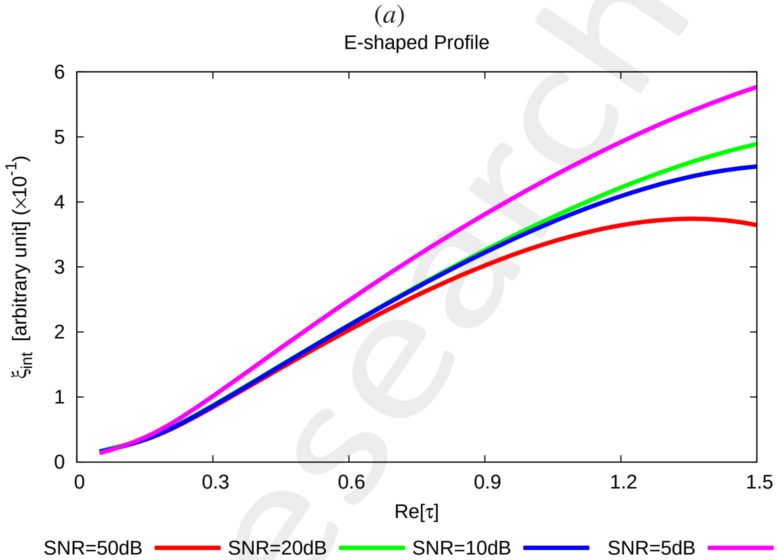

(b)

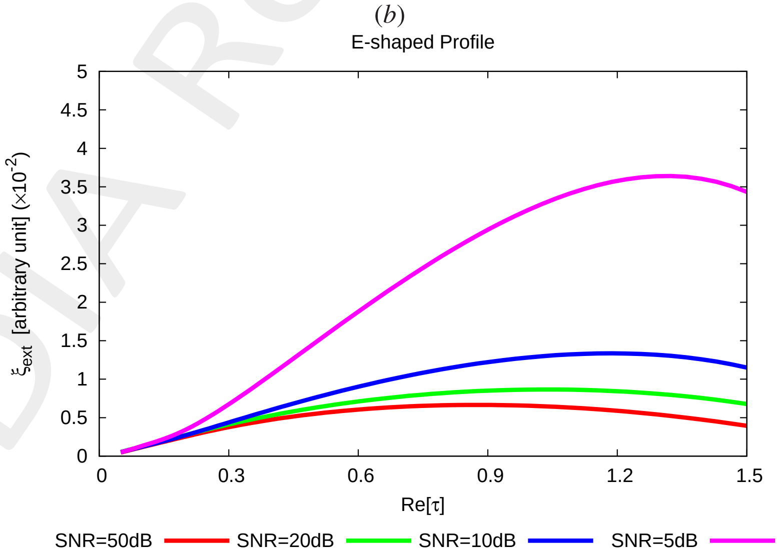

(c)

Figure 5: *E-shaped Object* - Reconstruction errors vs. τ: (a) total error, (b) internal error and (c) external error.

2.1.6 E-shaped Object, $\ell = 1.5\lambda$ - Resume: Errors vs. SNR

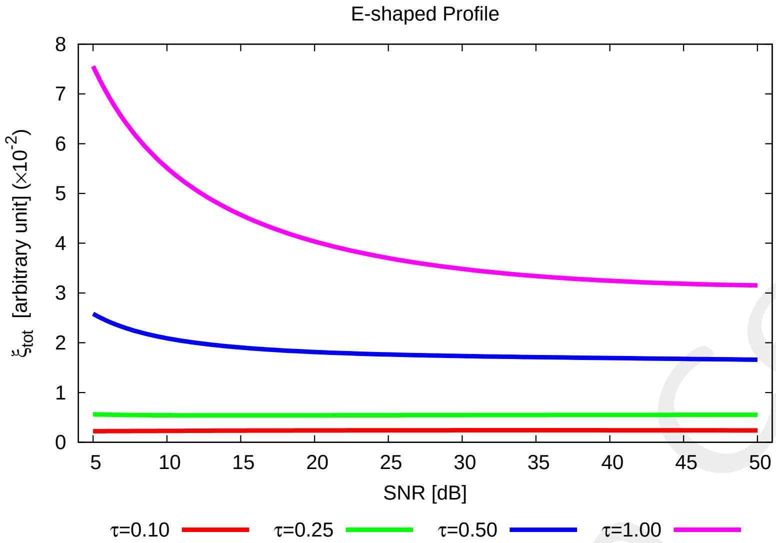

(a)

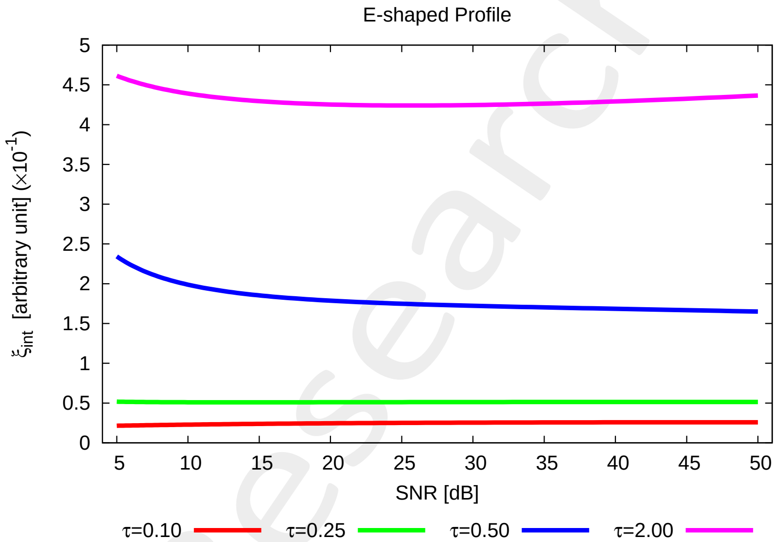

(b)

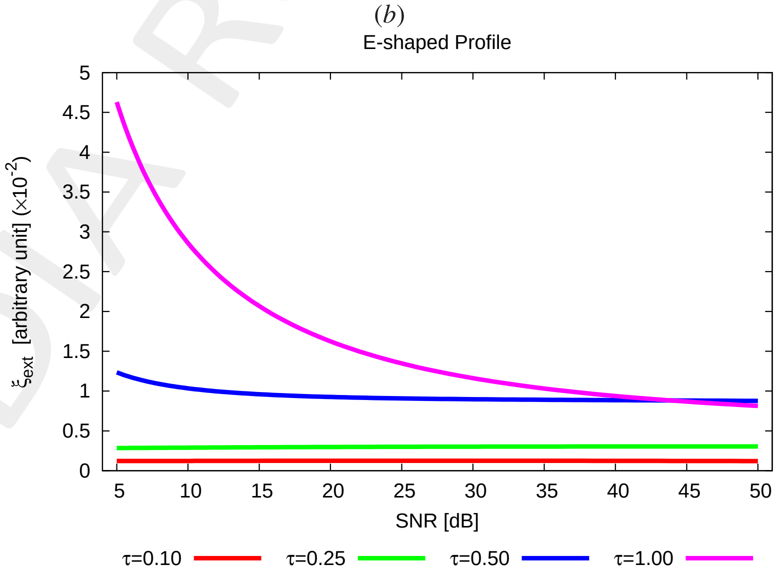

(c)

Figure 6: *E-shaped Object* - Reconstruction errors vs. SNR: (a) total error, (b) internal error and (c) external error.

2.1.7 E-shaped Object, $\ell = 1.5\lambda$ - Resume: Errors vs. $IMSA$ step, S

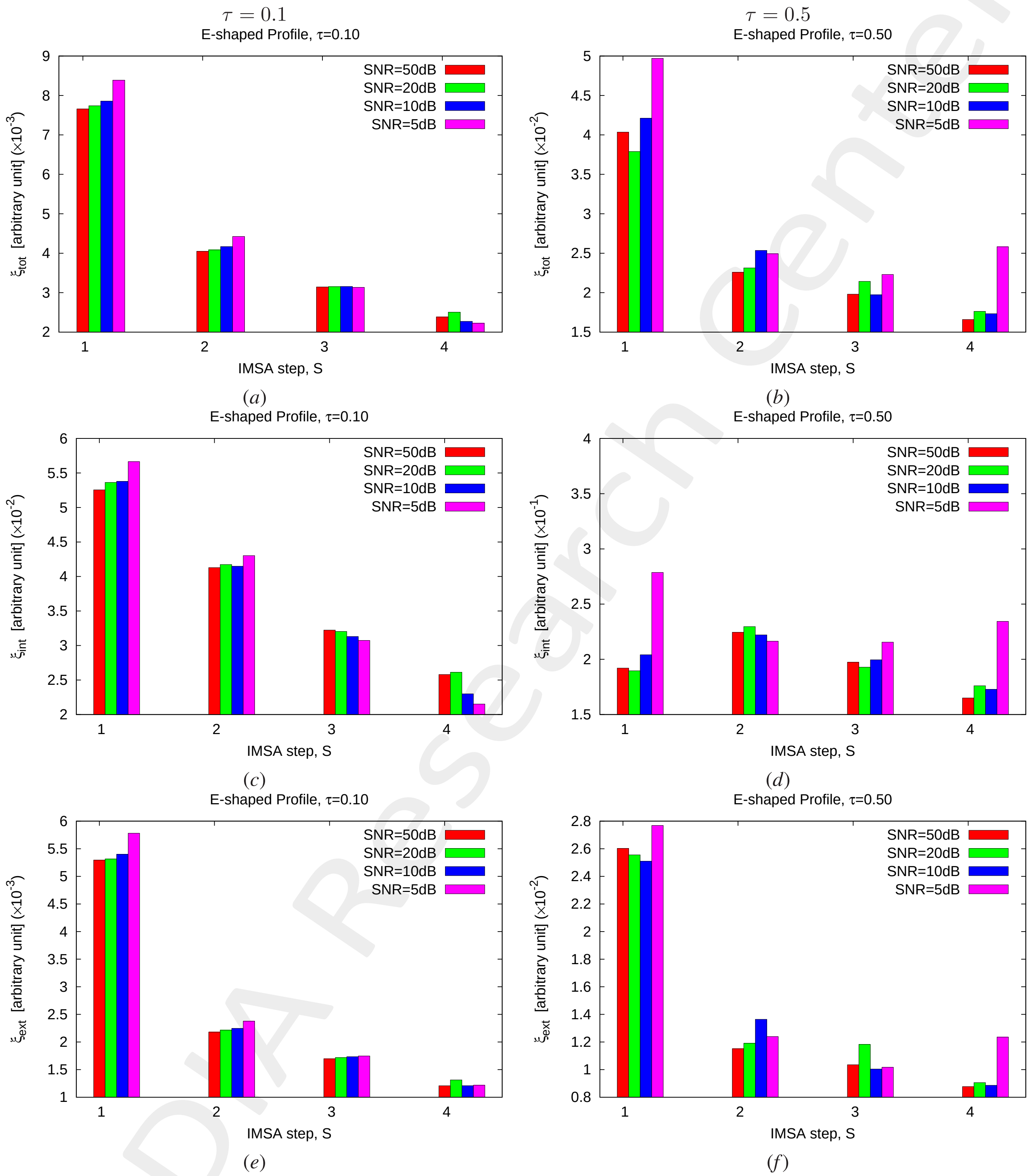

Figure 7: *E-shaped Object* - Reconstruction errors vs. $IMSA$ step, S: $(a)(b)$ total error, $(c)(d)$ internal error and $(e)(f)$ external error for $(a)(c)(e)$ $\tau = 0.1$ and $(b)(d)(f)$ $\tau = 0.5$.

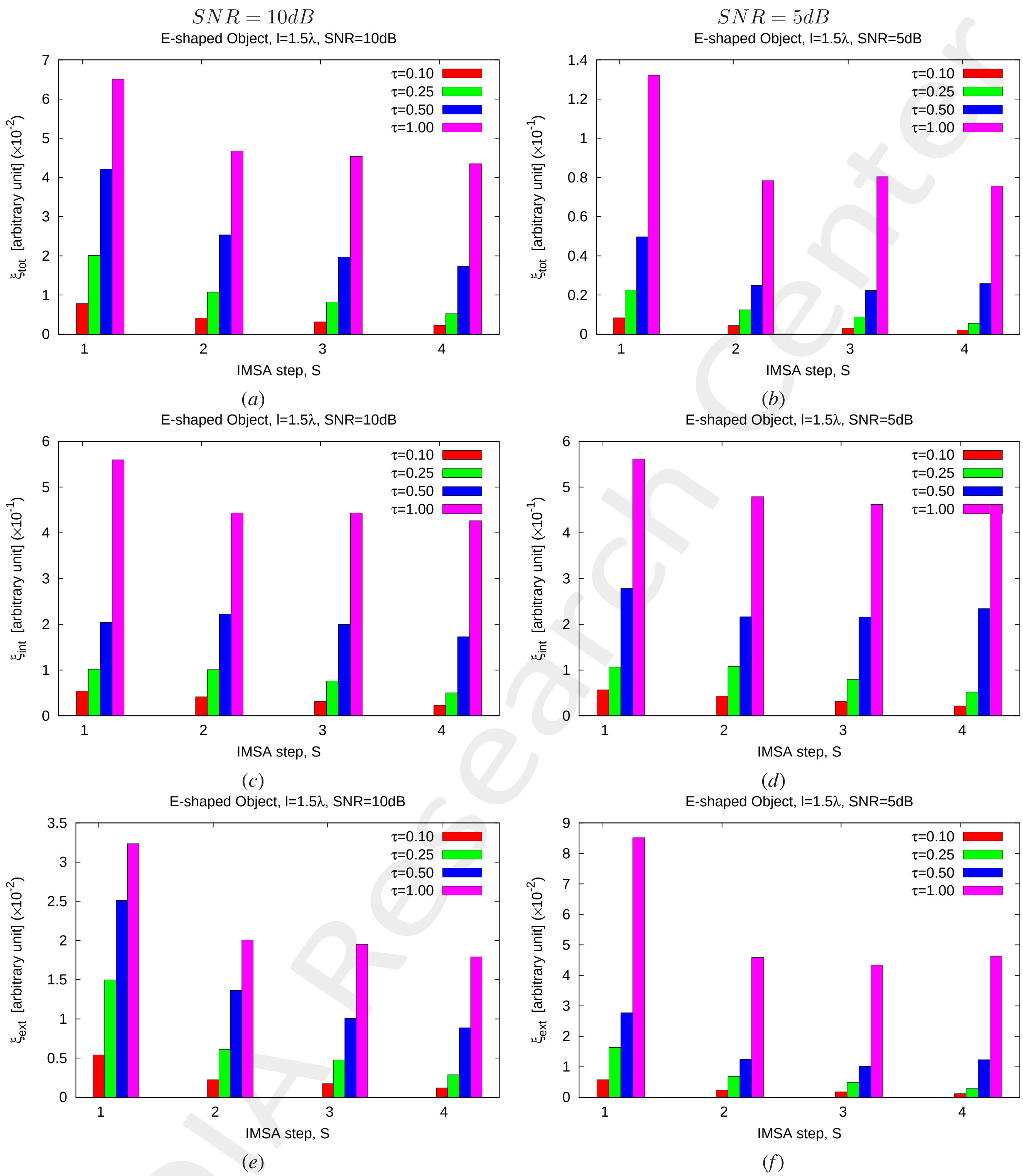

Figure 8: *L-shaped Object*, $\ell = 1.5\lambda$ - Reconstruction errors vs. $IMSA$ step, S: $(a)(b)$ total error, $(c)(d)$ internal error and $(e)(f)$ external error for $(a)(c)(e)$ $SNR = 10dB$ and $(b)(d)(f)$ $SNR = 5dB$.

More information on the topics of this document can be found in the following list of references.

References

[1] G. Oliveri, M. Salucci, N. Anselmi, and A. Massa, "Compressive sensing as applied to inverse problems for imaging: theory, applications, current trends, and open challenges," *IEEE Antennas Propag. Mag. - Special Issue on 'Electromagnetic Inverse Problems for Sensing and Imaging,'* vol. 59, no. 5, pp. 34-46, Oct. 2017 (DOI: 10.1109/MAP.2017.2731204).

[2] A. Massa, P. Rocca, and G. Oliveri, "Compressive sensing in electromagnetics - A review," *IEEE Antennas Propag. Mag.*, pp. 224-238, vol. 57, no. 1, Feb. 2015 (DOI: 10.1109/MAP.2015.2397092).

[3] A. Massa and F. Texeira, "Guest-Editorial: Special Cluster on Compressive Sensing as Applied to Electromagnetics," *IEEE Antennas Wirel. Propag. Lett.*, vol. 14, pp. 1022-1026, 2015 (DOI: 10.1109/LAWP.2015.2425011).

[4] M. Salucci, L. Poli, F. Zardi, L. Tosi, S. Lusa, and A. Massa, "Contrast source inversion of sparse targets through multi-resolution Bayesian compressive sensing," *Inverse Probl.*, vol. 40, no. 5, p. 055016, May 2024 (DOI 10.1088/1361-6420/ad3b33).

[5] G. Oliveri, N. Anselmi, M. Salucci, L. Poli, and A. Massa, "Compressive sampling-based scattering data acquisition in microwave imaging," *J. Electromagn. Waves Appl.* J, vol. 37, no. 5, 693-729, Mar. 2023 (DOI: 10.1080/09205071.2023.2188263).

[6] G. Oliveri, L. Poli, N. Anselmi, M. Salucci, and A. Massa, "Compressive sensing-based Born iterative method for tomographic imaging," *IEEE Tran. Microw. Theory Techn.*, vol. 67, no. 5, pp. 1753-1765, May 2019 (DOI: 10.1109/TMTT.2019.2899848).

[7] M. Salucci, L. Poli, and G. Oliveri, "Full-vectorial 3D microwave imaging of sparse scatterers through a multi-task Bayesian compressive sensing approach," *Journal of Imaging*, vol. 5, no. 1, pp. 1-24, Jan. 2019 (DOI: 10.3390/jimaging5010019).

[8] M. Salucci, A. Gelmini, L. Poli, G. Oliveri, and A. Massa, "Progressive compressive sensing for exploiting frequency-diversity in GPR imaging," *J. Electromagn. Waves Appl. J*, vol. 32, no. 9, pp. 1164-1193, 2018 (DOI: 10.1080/09205071.2018.1425160).

[9] N. Anselmi, L. Poli, G. Oliveri, and A. Massa, "Iterative multi-resolution bayesian CS for microwave imaging," *IEEE Trans. Antennas Propag.*, vol. 66, no. 7, pp. 3665-3677, Jul. 2018 (DOI: 10.1109/TAP.2018.2826574).

[10] N. Anselmi, G. Oliveri, M. A. Hannan, M. Salucci, and A. Massa, "Color compressive sensing imaging of arbitrary-shaped scatterers," *IEEE Trans. Microw. Theory Techn.*, vol. 65, no. 6, pp. 1986-1999, Jun. 2017 (DOI: 10.1109/TMTT.2016.2645570).

[11] N. Anselmi, G. Oliveri, M. Salucci, and A. Massa, "Wavelet-based compressive imaging of sparse targets," *IEEE Trans. Antennas Propag.*, vol. 63, no. 11, pp. 4889-4900, Nov. 2015 (DOI: 10.1109/TAP.2015.2444423).

[12] G. Oliveri, P.-P. Ding, and L. Poli, "3D crack detection in anisotropic layered media through a sparseness-regularized solver," *IEEE Antennas Wirel. Propag. Lett.*, vol. 14, pp. 1031-1034, 2015 (DOI: 10.1109/LAWP.2014.2365523).

[13] L. Poli, G. Oliveri, P.-P. Ding, T. Moriyama, and A. Massa, "Multifrequency Bayesian compressive sensing methods for microwave imaging," *J. Opt. Soc. Am. A*, vol. 31, no. 11, pp. 2415-2428, 2014 (DOI: 10.1364/JOSAA.31.002415).

[14] G. Oliveri, N. Anselmi, and A. Massa, "Compressive sensing imaging of non-sparse 2D scatterers by a total-variation approach within the Born approximation," *IEEE Trans. Antennas Propag.*, vol. 62, no. 10, pp. 5157-5170, Oct. 2014 (DOI: 10.1109/TAP.2014.2344673).